Geomechanics and Engineering, *Vol. 22, No. 3 (2020) 207-217*
DOI: https://doi.org/10.12989/gae.2020.22.3.207

Reliability and risk assessment for rainfall-induced slope failure in spatially variable soils

Liuyuan Zhao[1,2a], Yu Huang[*1,3], Min Xiong[1b] and Guanbao Ye[1,3c]

[1]Department of Geotechnical Engineering, College of Civil Engineering, Tongji University, Shanghai 200092, China
[2]PowerChina Huadong Engineering Corporation Limited, Hangzhou 311122, China
[3]Key Laboratory of Geotechnical and Underground Engineering of the Ministry of Education, Tongji University, Shanghai 200092, China

(Received September 29, 2019, Revised June 17, 2020, Accepted June 26, 2020)

Abstract. Slope reliability analysis and risk assessment for spatially variable soils under rainfall infiltration are important subjects but they have not been well addressed. This lack of study may in part be due to the multiple and diverse evaluation indexes and the low computational efficiency of Monte-Carlo simulations. To remedy this, this paper proposes a highly efficient computational method for investigating random field problems for slopes. First, the probability density evolution method (PDEM) is introduced. This method has high computational efficiency and does not need the tens of thousands of numerical simulation samples required by other methods. Second, the influence of rainfall on slope reliability is investigated, where the reliability is calculated from based on the safety factor curves during the rainfall. Finally, the uncertainty of the sliding mass for the slope random field problem is analyzed. Slope failure consequences are considered to be directly correlated with the sliding mass. Calculations showed that the mass that slides is smaller than the potential sliding mass (shallow surface sliding in rainfall). Sliding mass-based risk assessment is both needed and feasible for engineered slope design. The efficient PDEM is recommended for problems requiring lengthy calculations such as random field problems coupled with rainfall infiltration.

Keywords: slope risk assessment; rainfall-induced slope failure; random fields; spatially variable soil; probability density evolution method

1. Introduction

There are many variables that influence the slope stability. Uncertainties concerning the exact values for these variables lead to great challenges in slope stability analysis. The variables in slope stability analysis including site boundaries (Liu *et al.* 2017, Wang *et al.* 2017), variable soil strengths (Griffiths *et al.* 2009, Li *et al.* 2016a, Zhang and Huang 2016, Li *et al.* 2017, Chenari and Fatahi 2019), permeability coefficients (Zhang *et al.* 2005, Cho 2014, Jamshidi Chenari and Behfar 2017), and the varied coupling of multiple parameters (Zhang *et al.* 2014). Generally, the probabilistic approach is effective for solving uncertainty problems (Juang *et al.* 2015), for example, the random field for spatial variability problem (Vanmarcke and Erik 1983, Griffiths and Fenton 2004, Low *et al.* 2007, Griffiths *et al.* 2009, Qi and Li 2018, Zhu and Yang 2018).

The uncertainties mentioned above are mainly due to a lack of knowledge about the initial slope conditions. Different initial conditions may cause the slope to fail under different triggering factors, such as earthquake, rainfall, etc. Among the different types of landslides, rainfall-induced landslides commonly cause significant economic losses (Dai and Lee 2001, Dahal *et al.* 2008, Huang *et al.* 2015, Van Tien *et al.* 2018), and this type of landslide is recognized worldwide as a natural hazard (Zhang *et al.* 2014). For example, 82.15% of the fatal landslides mainly occurred between April and September in China (statistical time spans from 1950 to 2016), which is consistent with the monthly precipitation (Lin and Wang 2018). Thus, reliable analysis and risk assessment for rainfall-induced slopes failure in varied spatial orientations are very important problems.

However, these problems have not been well addressed. Much of the published research has not considered rainfall as a triggering factor on slopes composed of spatially variable soil. Examples include some research on slope reliability analysis (Low *et al.* 2007, Griffiths *et al.* 2009, Zhang *et al.* 2010, Juang *et al.* 2015, Jiang and Huang 2016), system reliability analyses (Huang *et al.* 2010, Jiang *et al.* 2014, Jiang *et al.* 2017a, Li *et al.* 2017, Liu *et al.* 2017), and risk assessments (Huang *et al.* 2013, Li and Chu 2016, Zhang and Huang 2016, Liu *et al.* 2017, Qi and Li 2018). In part, this lack of research on rainfall-induced slope failure in spatially variable soils is because incorporating the necessary rainfall time factors would increase computation times by several orders of magnitude.

To solve this problem, this paper investigates the

∗Corresponding author, Professor
E-mail: yhuang@tongji.edu.cn
[a]Ph.D.
E-mail: 1410270@tongji.edu.cn
[b]Ph.D.
E-mail: 1310298@tongji.edu.cn
[c]Professor
E-mail: ygb1030@126.com

ISSN: 2005-307X (Print), 2092-6219 (Online)

reliability and risk of rainfall-induced slope failure in spatially variable soils. This is done for slopes where the slope reliability can be determined based on the factor of safety (FOS) and the slope risk can be assessed based on sliding mass, which is directly related to the damage consequences of the landslide. This relationship has been recognized by many researchers (Juang *et al.* 2015, Li *et al.* 2016a, Liu *et al.* 2017) and verified after studying many landslide disasters (Staron and Lajeunesse 2009, Johnson *et al.* 2016, Xu *et al.* 2016, Yu *et al.* 2016). In addition, some preliminary studies have investigated the sliding mass-based risk assessments for slopes (Huang *et al.* 2013, Li and Chu 2016, Zhang and Huang 2016, Liu *et al.* 2017, Qi and Li 2018).

For some of the numerical methods used to investigate soil slopes with spatial variability problems, the computational tasks are very large. Especially for the limit equilibrium method (LEM), which requires a large number of potential sliding surfaces, and the Monte-Carlo method (Griffiths *et al.* 2009, Jiang *et al.* 2014, Jamshidi Chenari and Alaie 2015) that requires a large number of random samples (Li and Chu 2016). To improve the efficiency of the calculations and produce a more accurate probability density function distribution, this paper uses the probability density evolution method (PDEM) to investigate the slope reliability and risk assessment for spatially variable soils, which has provided a new framework for rainfall-induced slopes failure in spatially variable soil.

2. Methodology

2.1 Slope simulation with random fields

Based on the framework of random fields (Vanmarcke and Erik 1983) for the inherent spatial variability of soil (Elkateb *et al.* 2003), the Karhunen-Loève (K-L) expansion was used to simulate a two-dimensional slope with anisotropic random fields. This method was applied to generate anisotropic random fields using Eqs. (1)-(3). The realization of the random field was approximated by $\hat{H}(\mathrm{x},\theta)$ (Cho 2009). The equations are:

$$H(\mathrm{x},\theta)=\mu+\sum_{i=1}^{\infty}\sigma\sqrt{\lambda_i}\varphi_i(x)x_i(\theta),x\in\Omega \tag{1}$$

$$\int_{\Omega}\rho(x,x')\varphi_i(x')d\Omega_{x'}=\lambda_i\varphi_i(x) \tag{2}$$

$$\hat{H}(\mathrm{x},\theta)=\mu_{\mathrm{i}}+\sum_{i=1}^{N}\sigma_i\sqrt{\lambda_j}\varphi_j(x)x_{i,j}(\theta),(i=c,\phi) \tag{3}$$

where, Ω is the calculation domain, μ is the mean value of the random field, σ is the standard deviation, λ and φ are the eigenvalue and characteristic function of the autocorrelation function, respectively, x and x' are the coordinates of one dimensional, ρ is the autocorrelation function, $\widehat{H}(x,\theta)$ is the approximate random field of $H(x, \theta)$, N is the number of K-L terms (where N = 150 in this paper), c and ϕ are the cohesion and internal friction angle of soils, respectively.

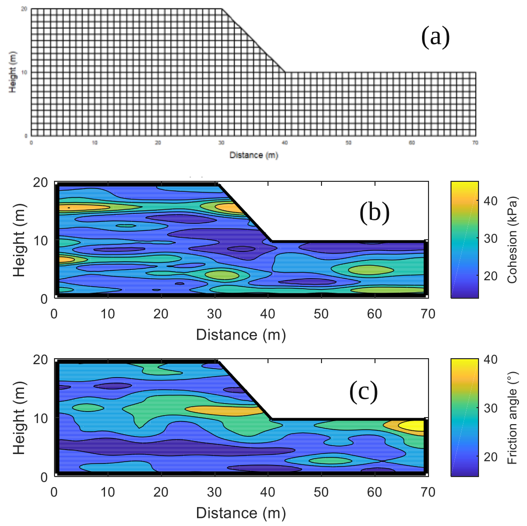

Fig. 1 Schematic representation showing slope models for (a) material regions; typical realizations of random field, (b) cohesion and (c) internal friction angle

In the anisotropic random fields, an exponential autocorrelation function was used. Thus, the realized $\widehat{H}(x,\theta)$ should be converted to the standard state by Eq. (4). Eq. (5) shows the exponential autocorrelation function in two-dimensional space (Cho 2009).

$$\hat{H}(\mathrm{x},\theta)=\exp[\mu_{\mathrm{i}}+\sum_{i=1}^{N}\sigma_i\sqrt{\lambda_j}\varphi_j(x)x_{i,j}(\theta)],(i=c,\phi) \tag{4}$$

$$\rho(x,y)=\exp(-\frac{|x-x'|}{l_h}--\frac{|y-y'|}{l_v}) \tag{5}$$

where l_h and l_v are the autocorrelation distances in the horizontal and vertical directions, respectively, x and x', y and y' are the coordinates in the two-dimensional random field. Other parameters can be referred in Eqs. (1)-(3).

To realize the random field for the soil slope, the slope regions need to be divided for the different materials. Fig. 1(a) shows the material regions for the slope random field; there are total of 1,055 regions each rectangular region being 1 m by 1 m in size. Fig. 1(b) shows a typical realization for a common random field model (Cho 2009), where l_h = 20 m, l_v = 2 m, ρ(c, φ) = −0.5, mean c = 20 kPa, mean φ = 25°, coefficient of variation of cohesion (COVC) = 0.3, coefficient of variation of friction angle (COVF) = 0.2. It can be seen by comparing Fig. 1(b) with Fig. 1(c) that the soil's cohesion and internal friction angles are negatively correlated and that the random fields are well realized.

2.2 Hydraulic characteristics

For saturated soils, the hydraulic conductivity is constant but for unsaturated soils, the hydraulic conductivity depends on the degree of saturation or the matric suction. For this study, the Van Genuchten model (Van Genuchten 1980) was used to define the hydraulic characteristics. Using this model, the hydraulic conductivity can be calculated from the matric suction and the volumetric water content using Eqs. (6) and (7) (Van Genuchten 1980):

$$\Theta = \frac{\theta - \theta_{\mathrm{r}}}{\theta_s - \theta_{\mathrm{r}}} = [\frac{1}{1+[\alpha(u_a - u_w)]^n}]^{1-1/n} \tag{6}$$

$$k = k_s \Theta^{1/2}[1-(1-\Theta^{1/(1-1/n)})^{1-1/n}]^2 \tag{7}$$

where, Θ is the normalized volumetric water content or effective water saturation, θ, θ_r and θ_s are the volumetric water content, residual water content, and saturated volumetric water content, respectively, k is the hydraulic conductivity of the unsaturated soil, u_a is the pore air pressure, u_w is the pore water pressure, k_s is the saturated hydraulic conductivity, and α and n are fitting parameters for the model (Van Genuchten 1980).

2.3 Probability density evolution method

The PDEM is a highly efficient stochastic analysis method because it can quickly approximate an analytic solution for the probability density function (Li and Chen 2008, 2009, Chen and Li 2009). The core of the method is the probability conservation principle, which means the total probability remains unchanged in a conservative system. For slope stability problems, by solving the slope stability balance equation on the basis of existing deterministic methods, any physical parameters (e.g. the displacement or safety factor) can be chosen as the random variable in the PDEM equation. The one-dimensional PDEM equation can be written as Eq. (8) (Chen and Li 2009):

$$\frac{\partial p_{H\Theta}(h,\theta,t)}{\partial t} + \sum_{j=1}^{m} \dot{H}_j(\theta,t)\frac{\partial p_{H\Theta}(h,\theta,t)}{\partial h_j} = 0 \tag{8}$$

where H is composed of physical quantities and Θ is a random vector. The variable $p_{H\Theta}$ is the joint probability density function, θ is the basic random variable, and t is the time for the physical process.

In Eq. (8), if the physical quantity is FOS, it can be written as Eq. (9), a similar analysis of slope has been published by the authors (Huang and Xiong 2017, Huang *et al.* 2018, Hu and Huang 2019). Eq. (9) is written as:

$$\frac{\partial p_{F\Theta}(F,\theta,t)}{\partial t} + \dot{F}(\theta,t)\frac{\partial p_{F\Theta}(F,\theta,t)}{\partial F} = 0 \tag{9}$$

where F is the FOS.

To solve Eq. (9), the representative discretized points in the two-dimensional basic random variable space Θ should be selected firstly (the points for soil cohesive and internal friction angle in a random field) and the initial probability of each sample should be assigned. For this paper, these values were obtained using the sphere packings method, which is a smart way to determine the representative points and useful for the PDEM (Chen and Li 2009). Fig. 2 shows the point selection method in two-dimensional standard normal space. In Fig. 2(a) the red circle denotes $X_1^2 + X_2^2$ $\leq 3.5^2$. Using this method, the coordinates of the selected points are random variables. The points were selected from center to the edge and the assigned probabilities gradually decrease, as shown in Fig. 2(b). Each point occupies the same area in standard normal space and the occupied areas were calculated according to hexagonal equivalence, thus the hexagonal outline in Fig. 2(a). For this paper, 469 points in two-dimensional standard normal space were selected. This number of points is adequate to provide the required accuracy and guarantees that there are a sufficient number of failure cases for the PDEM.

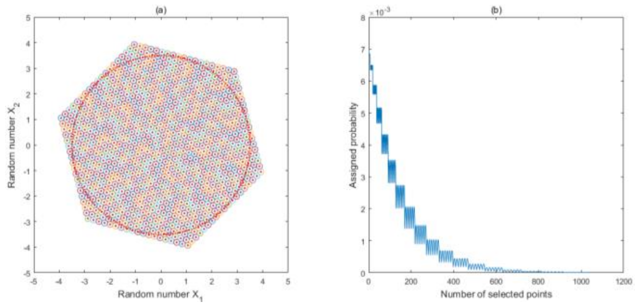

(a) (b)

Fig. 2 Illustration showing representative points determined by the sphere packings method; (a) the distribution of random numbers in 2-D normal space and (b) the corresponding assigned probabilities

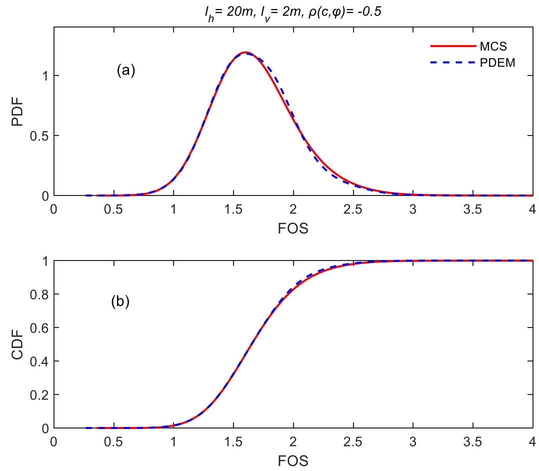

Fig. 3 Graphs comparing FOS distributions (a) PDF and (b) CDF determined by MCS and PDEM for a slope with spatially varied soil. FOS = factor of safety, PDF = probability density function, CDF = cumulative probability function. See the text for the slope's physical and mechanical parameters

3. Verification of PDEM for spatially variable soil analysis

Generally, the calculations required for Monte-Carlo simulation (MCS) of random field problem are extremely time-consuming. For example, to solve for a slope with spatially variable soils, 23,000 realizations by Li *et al.* (2016b) and 50,000 realizations by Cho (2009) were

Table 1 Parameter settings for the spatially varied soil random fields

Parameters	Value
γ_d (kN/m^3)	17
l_h (m)	20
l_v (m)	2
ρ (c, φ)	-0.5
mean c (kPa)	8
mean φ (°)	25
COVC	0.15
COVF	0.1

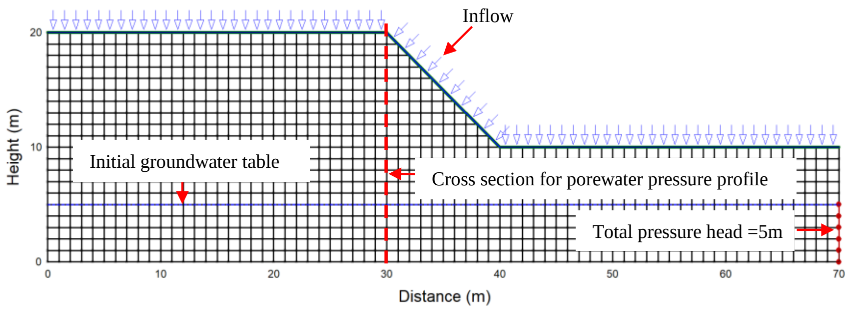

Fig. 4 Diagram showing the initial settings for the rainfall infiltration numerical model

required. However, using PDEM, only several hundred samples are necessary and the results are very similar to MCS results (Li and Chen 2009).

To illustrate the efficiency and accuracy of PDEM, Fig. 3 shows a comparison of FOS distributions in a slope with spatially variable soil as determined by MCS and PDEM. Fig. 3 shows 10,000 realizations by MCS and 469 realizations by PDEM based on random fields. The case used in the figure is a common slope (Cho 2009) with the parameters slope height = 10 m, slope angle = 45°, l_h = 20 m, l_v = 2 m, ρ(c, φ) = −0.5, mean c = 20 kPa, mean φ = 25°, COVC = 0.3, COVF = 0.2, and γ = 17.8 kN/m^3. It can be seen that the FOS distributions are nearly identical. The relative CDF errors are 0.4% (FOS = 1.5) and 1.78% (FOS = 2.0).

4. Slope model parameter settings

4.1 Slope geometry and soil spatial variability

Jiang and Huang (2016) summarized the published researches on random field problems and found that the slope most commonly modeled by these investigations was 10 m high with a slope angle of 45 degrees. Therefore, a soil slope with a height of 10 m high and 1 m wide (2D slope for the sliding mass calculations) was used in this paper. The calculation boundary width is three times the height of the slope and the bottom thickness is equal to the slope height. The slope's physical and mechanical parameters are the same as those specified for the verification case described above. A similar model was used to carry out slope testing by Huang and Xiong (2017).

There are three methods that can be used to solve for slope stability when the slope incorporates spatially variable soil. They are the random finite element method (RFFM), the random finite difference method (RFDM), and the random limit equilibrium method (RLEM). Many scholars have used (Cho 2009, Huang *et al.* 2013 Jiang *et al.* 2017b, Qi and Li 2018) or proposed improvements on RLEM (Zhang and Huang 2016, Javankhoshdel *et al.* 2018, Izadi *et al.* 2020, Mafi *et al.* 2020) in their researches. In addition, the obtained FOSs by RLEM and RFEM were found to be very similar (Griffiths and Lane 1999, Cala and Flisiak 2001, Griffiths and Fenton 2004, Ozbay and Cabalar 2015). Moreover, some optimization methods based on RLEM, such as surface altering optimization has been demonstrated to show a good accuracy and speed (Mafi *et al.* 2020). Thus, the RLEM was used for this investigation.

For RLEM, the number of potential slip surfaces is very important. Too few slip surfaces will not allow the method to represent all the potential variability in the sliding mass, but too many surfaces will make the calculations excessively complex and time-consuming. Previous researchers have used more than 5,000 potential sliding surfaces. For example Jiang *et al.* (2017b) used 5,551 slip surfaces, Zhang and Huang (2016) used 9,200–15,000 slip surfaces, and 16,400 surfaces were used in the calculations presented by Li *et al.* (2016b). For this paper, a total of 5,887 potential slip surfaces were generated in area encompassing 1.5 times the slope height. The final results show that this number of surfaces is reasonable because all the critical slip surfaces are in this area.

Table 1 shows the parameters for the random field based on Cho (2009, 2014), where the mean soil cohesion and internal friction angle is based on Rahardjo *et al.* (2007) and the soil's properties are similar to the silt described by Lee *et al.* (2009) and Yang *et al.* (2018). It should be pointed out

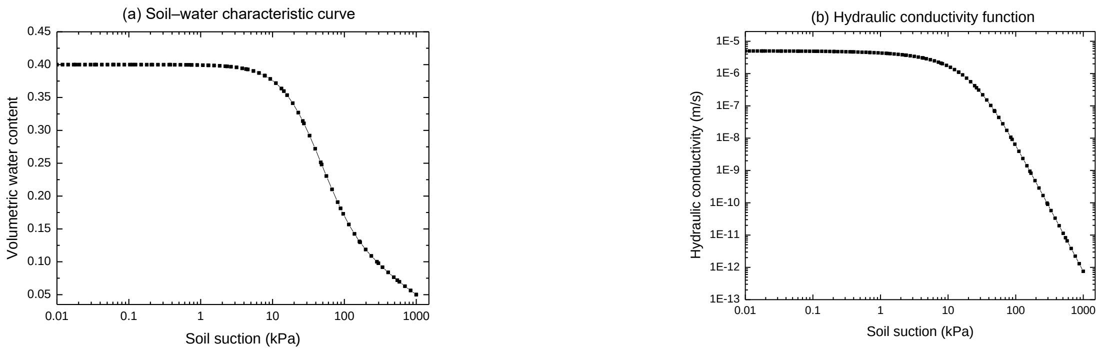

Fig. 5 Graphs showing the hydraulic characteristics of the model soil. (a) Soil-water characteristic curve and (b) Hydraulic conductivity curve. Note: This figure is based on the model proposed by Van Genuchten (1980)

Table 2 Parameters used to construct the soil water characteristic curve shown in Fig. 5

Parameters	Value
θ_s	0.40
θ_r	0.04
α (kPa $^{-1}$)	0.1
n	2
k_s (m/s)	5×10^{-6}

Table 3 Rainfall intensities, durations, and analysis times used in the numerical simulations

Case	Intensity (mm/h)	Duration (h)	Total analysis time (h)
Case 1	10	24	72
Case 2	80	24	72
Case 3	80	3	72

that all the slope samples should be stable (to ensure the slope samples have the engineering meanings) before the rainfall begins (initial FOS > 1), which means that the setting of coefficient of variation for the soils is not very high.

4.2 Rainfall and hydraulic parameter settings

Fig. 4 shows the configuration and hydraulic boundary conditions for the rainfall infiltration model. The initial water table depth is five meters below the elevation of the foot of the slope and the phreatic seepage boundary was set at the right side of the model (with a constant total pressure head). The groundwater flow analyses require an initial condition, and the initial maximum negative pressure was set of 50 kPa based on Rahardjo *et al.* (2007).

Fig. 5 shows the soil water characteristic curve (SWCC) for the soil in the slope. The curve is based on the Van Genuchten model (Van Genuchten 1980) and the soil is similar to silt (Lee *et al.* 2009, Rahardjo *et al.* 2007, Yang *et al.* 2018). The values for the parameters used to construct Fig. 5 are listed in Table 2.

A large amount of field data and numerous research projects have shown that one of the most important factors involved in causing rainfall-induced landslides are rainfall duration and intensity (Guzzetti *et al.* 2008, Galanti *et al.* 2018, Segoni *et al.* 2018). Generally, rainfall intensity is 10-80 mm/h and the rainfall duration can range from a few minutes to several days. Example intensities reported in the literature include 10.8 mm/h (Cho 2014), 7.2-43.2 mm/h (Zhang *et al.* 2014), 14.5 mm/h (Yang *et al.* 2018), and extreme major rainfall of 9.12-89 mm/h (Lee *et al.* 2009). Table 3 lists three sets of rainfall intensity and duration data used to define three rainfall cases that were analyzed using the Seep/W groundwater flow analysis software from GEO-SLOPE (GEO-SLOPE International Ltd. 2018). The rainfall data used were similar to data used by the researchers mentioned above and the rainfall parameters recommended by the Seep/W documentation. Similar cases can be found on the Geoslope website (GEO-SLOPE International Ltd. 2018). The specific cases analyzed are: Case 1, intensity = 10 mm/h, duration = 24 h (long-term low-intensity rainfall); Case 2, intensity = 80 mm/h, duration = 24 h (long-term high-intensity rainfall); Case 3, intensity = 80 mm/h, duration = 3 h (short-term high-intensity rainfall). The analysis time for each of the three cases was 72 h (Table 3).

5. Reliability analysis and risk assessment

5.1 Reliability analysis

For slope reliability analysis, the first field that must be calculated is the rainfall infiltration and seepage. Fig. 6 shows the pore water pressure–height profiles for the three different rainfall cases in the slope shown in Fig, 4; the profiles are based on the SWCC curve in Fig 5. The initial maximum negative pressure in the soil for these profiles is 50 kPa, thus when the rain starts to fall, the pore water pressure in the soil near the surface gradually rises from −50 kPa.

As can be seen for Case 1 shown in Fig. 6(a), (low rainfall intensity for 24 h), seepage does not saturate the soil on the upper part of the slope until the rainfall ends. The groundwater level (model height = 5 m) does not increase and the water from the rainfall only influences the soil to a depth of about 5 m. However, for Case 2 shown in Fig. 6(b), the high rainfall intensity for 24 h causes the surface soil to be rapidly saturated and the groundwater level rises significantly. The maximum rainfall influence depth for this intense rainfall is about 9 m. For Case 3 in Fig. 6(c),

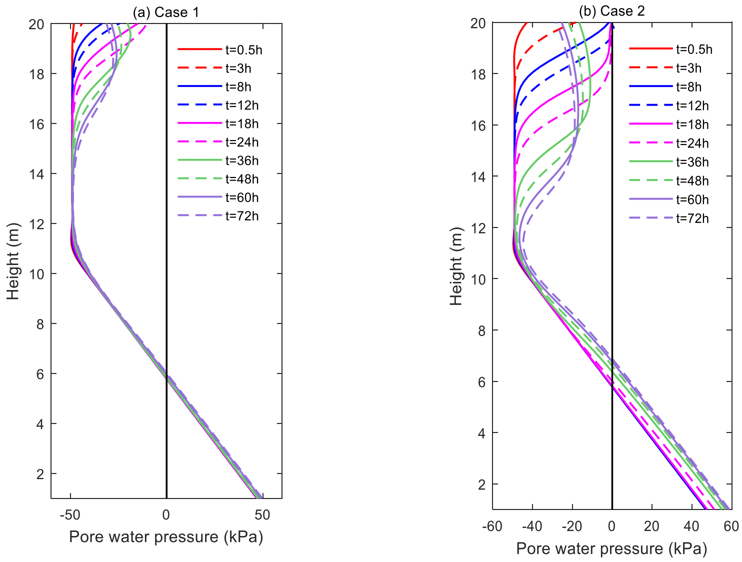

Fig. 6 Pore water pressure-height profiles for the three rainfall cases. (a) Case 1, (b) Case 2 and (c) Case 3. The rainfall intensity and duration for each case are listed in Table 3

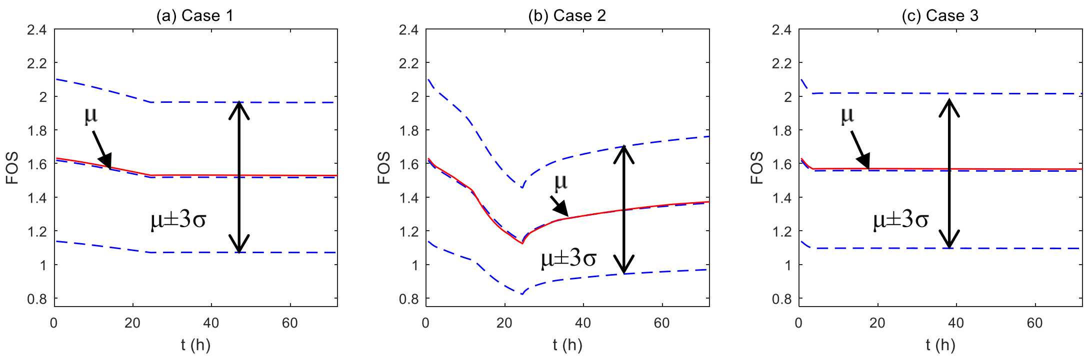

Fig. 7 Mean FOS vs. time curves for the three rainfall cases with FOS ± three standard deviations shown by the dashed lines. (a) Case 1, (b) Case 2 and (c) Case 3. The red lines are the slopes of the FOS curves with no random factor

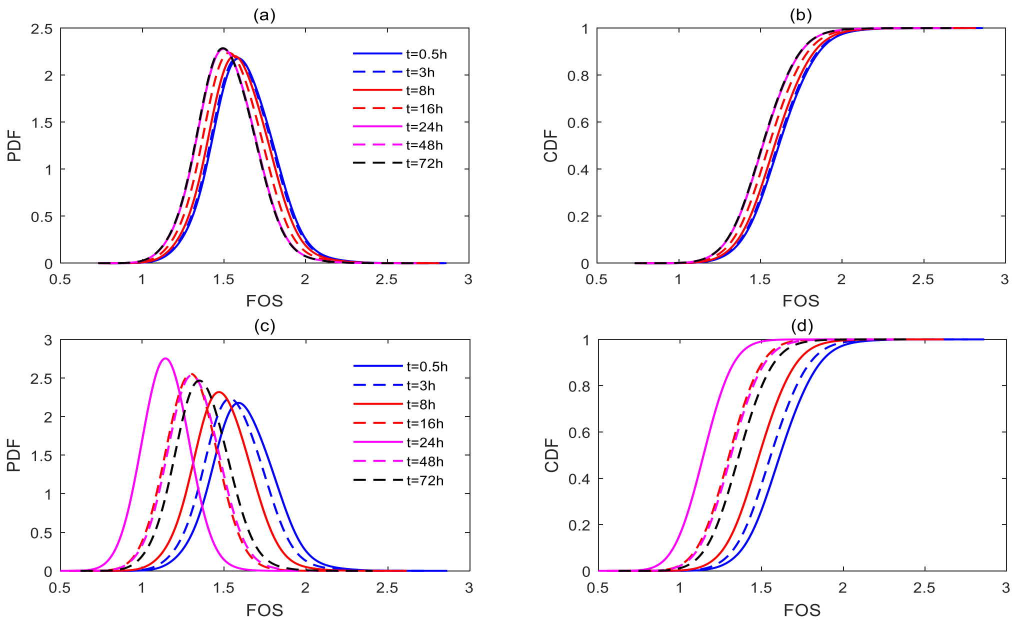

Fig. 8 Graphs showing probability density functions and cumulative probability functions vs. FOS for the three rainfall cases at different times. Case 1 - (a) and (b), Case 2 - (c) and (d) and Case 3 - (e) and (f)

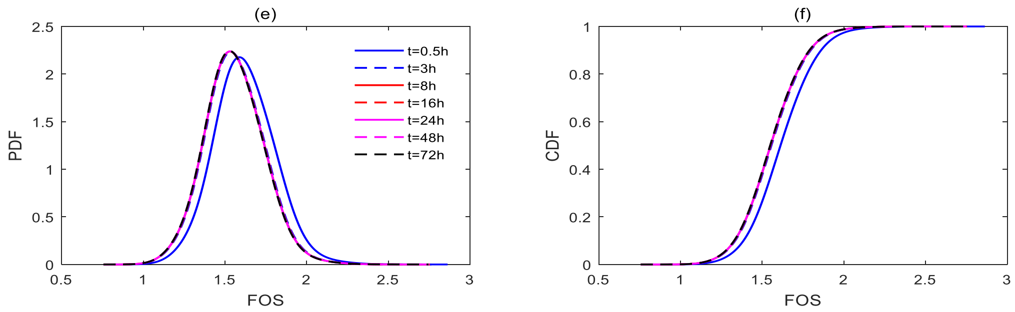

Fig. 8 Continued

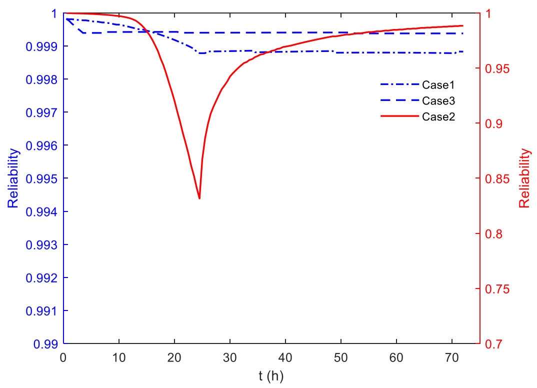

Fig. 9 Graph showing the reliability changes during rainfall for the three cases. The reliabilities for Case 1 and Case 3 are indicated on the left axis, the reliability for Case 2 on the right axis

although the total amount of water in the rainfall is the same as the rainfall in Case 1, the infiltration curve is quite different, and the maximum rainfall influence depth is about 5 m.

Rainfall infiltration leads to changes in the soil's shear strength, and the safety factor should be calculated by the unsaturated shear strength (Vanapalli *et al.* 1996). Eq. (10) is the shear strength equation suggested for unsaturated soils by Vanapalli *et al.* (1996):

$$\tau = c' + (\sigma_n - u_a)\tan\phi' + \Theta(u_a - u_w)\tan\phi' \qquad (10)$$

where τ is the shear strength, c' is the effective cohesion, σ_n is the total normal stress, u_a is the pore air pressure, u_w is the pore water pressure, ϕ' is the effective friction angle, and Θ is the normalized volumetric water content from Eq. (6).

For the model slope, the slope's FOS was calculated using the modified shear strength with the initial cohesion and internal friction angle parameters taken from the random field model described in the section of random fields. Then FOS values for each time period were calculated. Fig. 7 shows the mean FOS versus time curves and the curves for FOS plus and minus three times the standard deviation for the three rainfall cases. The red lines in Fig. 7 mark the slope of the FOS curves with no random factor and it is clear that the red lines are almost coincide with the mean FOS curves. This means the FOS curve slopes with no random factor are equivalent to the mean FOS curves that include the spatially variable soils.

To illustrate the effects of rainfall on the slope stability more clearly, Fig. 8 shows the probability density functions and the safety factors for the three rainfall cases at different times. The initial safety factor presents a normal distribution; the shapes of the curves result from the spatial variations in the soil's mechanical parameters. For low-intensity rainfall and short-term high-intensity rainfall, Cases 1 and 3, the PDF of the FOS moves to the left in Figs. 8(a) and 8(e), but the curves do not move very far (the change in PDF is not large). Note that the PDF's become stable after the rainfall ceases. However, for the long-term high-intensity rainfall, Case 2, the decrease in PDF is considerable (Fig. 8(c)). After 24 h, a significant proportion of the slope cases show slope failure. However, note that after the rainfall has ended at 24 h, the PDF of FOS moves back to the right (as shown by the t = 48 h and t = 72 h curves) which means that slope stability has been recovered.

Slope reliability can be calculated from $P_r = 1 - pf$, where P_r is reliability and pf is failure probability. For stochastic analysis, the value of CDF when FOS = 1 in Fig. 8 can be taken as the failure probability. The slope reliabilities during the rainfall were calculated and are shown in Fig. 9. Fig. 9 uses two Y-axes because the change in pf for Cases 1 and 3 are very small. However, the rainfall causes a significant change in slope reliability for Cases 2. During this rainfall, the reliability decreases rapidly after the rain has been falling for twelve hours, but after the rainfall, the reliability gradually recovers. Fig. 6 can be used to explain the differences in Fig. 9; a local saturation zone was generated around the slope surface during the rainfall (case 2), which will change into unsaturated seepage after rainfall. However, the slope surface never saturated during the rainfall for case 1 and case 3 (Fig. 6). Thus, no recovery phenomenon occurred.

In conclusion, when the spatial variations in the soil are considered, the reliability of slopes will be reduced significantly when the slope is subjected to long-term high-intensity rainfall. This is completely different from the results of deterministic analysis when the spatial variations in the soil are not considered (in Fig 7(b), the minimum FOS >1 for the long-term high-intensity rainfall). This difference arises because the initial safety factors for some portions of the slope are low when the spatial variations in the soil composition are taken into account; the rainfall can easily trigger a landslide in those parts of the slope. Therefore, considering the spatial variations in the soil when it rains is a more reasonable approach

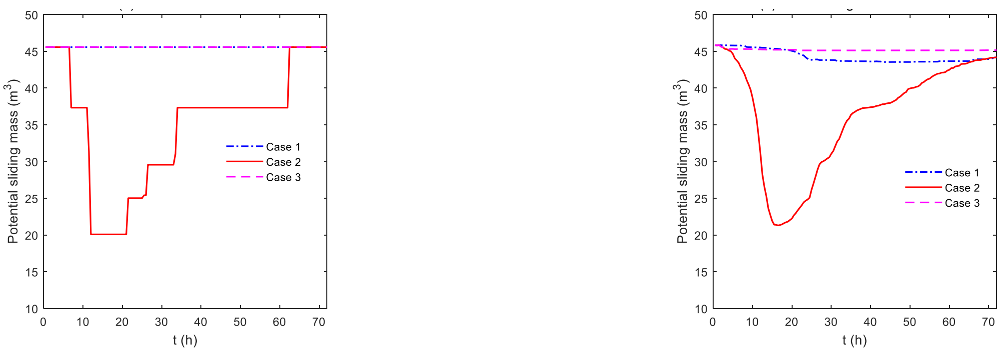

(a) No random factors (b) Considering the random factors

Fig. 10 Graphs showing the potential changes in sliding volumes during the three rainfall events with (a) no random factors and (b) considering the random factors. Note that none of the cases illustrated resulted in slope failure

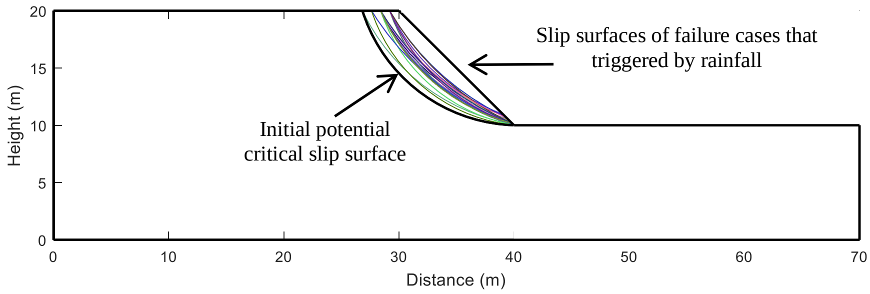

Fig. 11 Schematic representation showing slip surfaces in a landslides triggered by long-term high-intensity rainfall

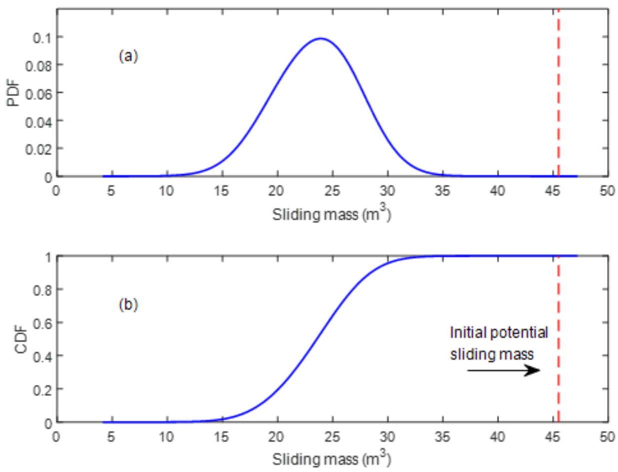

Fig. 12 Graphs showing the (a) PDF and (b) CDF vs. the sliding mass (for risk assessment) for high rainfall intensity induced landslide based on the slope failure cases

for the slope design engineering.

5.2 Risk assessment

Slope reliability and risk assessment are different but coupled. The distribution of safety factor for potential slip surfaces can be used for reliability analysis, and the sliding mass itself is a major part of the risk assessment. Risk assessments are generally related to the hazard, which refer to the likelihood of possible negative effects on infrastructure, structures, people and their belongings (Fenton and Griffiths 2008). The overall risk can be calculated using Eq. (11) if the consequences of the landslide are considered to be directly related to the sliding mass (Huang *et al.* 2013). A simplified form of Eq. (11) can be written as:

$$R = p_f \times C \tag{11}$$

where R is the risk, p_f is failure probability and C represents the consequences of the slope failure.

As mentioned previously, there are many methods for assessing the risk of soil slope failure. For this study, the method based on sliding masses was used. This method correlates the failure modes with the consequences and the total risk is taken to be the sum of all the individual failure risks. Using this approach, Eq. (11) should be rewritten as Eq. (12) (Huang *et al.* 2013):

$$R = \sum_{i=1}^{n_f} p_{fi} \times C_i \tag{12}$$

In engineering, the slope failure risk can be correlated with economic losses, and the C_i in Eq. (12) can be calculated from Eq. (13) (Liu *et al.* 2017):

$$C_i = \begin{cases} u_p V_i & g(X) \le 0 \\ 0 & g(X) > 0 \end{cases} \tag{13}$$

$$g(X) = \min[FOS(all)] - 1 \tag{14}$$

where, u_p is the unit price of economic losses, i is the computed failure cases, V_i is the sliding mass of failure samples, $g(X)$ is the performance function of slope, "$FOS(all)$" means all the potential sliding surfaces.

In Eq. (13), the consequence is proportional to the sliding mass and the variable u_p is unit price of the economic loss. However, the actual losses may differ by two orders of magnitude (Klose *et al.* 2015, Yin *et al.* 2016, Liu *et al.* 2017). Thus for this study, the slope risk assessment does not consider the economics but only analyzes the sliding mass uncertainty, which is feasible and reasonable (Li *et al.* 2016a, Zhang and Huang 2016).

A simplified illustration of the potential sliding mass volumes with no random factor is shown in Fig. 10(a). It can be seen in Fig. 10(a) that the potential sliding masses in Case 1 and Case 3 (the low-intensity rainfall and short-term high-intensity rainfall cases) do not decrease when the random factors are not considered. However, the long-term high-intensity rainfall, Case 2, leads to a significant reduction of the potential sliding mass. Although the slope does not fail in Case 2 (FOS > 1 in Fig. 7), the critical slip surface does gradually move towards the shallow surface, and the potential sliding mass also decreases. This may be because the soil near the slope's surface becomes saturated. Fig. 10(b) shows the mean curves for the potential sliding masses for the three rainfall cases when the variability in the slope parameters are considered. It can be seen that the critical sliding surface changes very little during the low-intensity rainfall and short-term high-intensity rainfall events. However, during the long-term high-intensity rainfall, the slope failure mechanism is moving towards shallow sliding. As pointed out in the discussion accompanying Fig. 8, the slope in Case 2 returns to its original state about two days after the rainfall ends. It should be pointed out that the Fig. 10(b) only shows the results that not failure for Case 2, and the failure samples under long-term high-intensity rainfall were illustrated and analyzed in Figs. 11 and 12.

Since low-intensity rainfall and short-term high-intensity rainfall did not cause slope failure when considering the variability of soil, Fig. 11 shows only the slip surfaces of landslides that triggered by long-term high-intensity rainfall. Clearly, the rainfall-induced slope failure mechanism was shallow sliding. The probability distribution for the sliding mass for the failure samples is shown in Fig. 12. For Fig. 12, the sliding masses were obtained based on the location of the slip surfaces at the time of slope failure. As can be seen from Fig. 12, the range of sliding masses is about 10-35 m^3 with a mean value of about 23 m^3. This mean is approximately half of the initial potential sliding mass.

Although the sliding masses obtained in Fig. 12 is not large, the analysis framework proposed in this paper shows its engineering application meanings, which including the variability of unstable volume, the distribution pattern caused by rainfall, the position of sliding surfaces, etc. Moreover, the risk assessment coupled failure probability and the sliding consequence analysis seem more reasonable than reliability analysis, thus it is suggested that the volume of the sliding mass be used for slope risk assessment. In addition, under long-term high-intensity rainfall, it has been shown that the sliding mass presents a normal distribution when the spatial variability of the soil is considered.

6. Conclusions

This study investigated the slope risk for slopes in spatially variable soils under rainfall. Several conclusions can be drawn.

• For slopes incorporated spatial variability problem, the probability density evolution method has a higher computational efficiency than Monte-Carlo simulations. This observation provides a new algorithm for investigating slope random field problems.

• For slope random field problems, slope reliability changes during rainfall. For low-intensity rainfall and short-term high-intensity rainfall, the decrease of reliability is small but for long-term high-intensity rainfall, the reliability decreases considerably. The reliability decreases because some of the initial slope safety factors are low when the spatially variable soils are considered and rainfall can easily trigger a landslide for this part of the slope samples.

• The risk assessment coupled failure probability and the sliding consequence analysis seem more reasonable than slope reliability analysis. Thus, the sliding mass-based risk assessment for slopes with spatially variable soils is recommended. During long-term high-intensity rainfall, the sliding mass presents a normal distribution when the spatial variability of the soil is considered, and the sliding mass is much smaller than the initial potential sliding mass, showing a shallow surface sliding mechanism.

Acknowledgments

This work was supported by the National Natural Science Foundation of China (Grant Nos. 41831291 and 41625011) and the National Key R&D Program of China (Grant No. 2017YFC1501304).

References

Cala, M. and Flisiak, J. (2001), "Slope stability analysis with FLAC and limit equilibrium methods", *Proceedings of the 2nd International FLAC Symposium*, Melbourne, Australia, February.

Chen, J.B. and Li, J. (2009), "A note on the principle of preservation of probability and probability density evolution equation", *Prob. Eng. Mech.*, **24**, 51-59. https://doi.org/10.1016/j.probengmech.2008.01.004.

Chenari, R.J. and Fatahi, B. (2019), "Physical and numerical modelling of the inherent variability of shear strength in soil mechanics", *Geomech. Eng.*, **17**(1), 31-45. https://doi.org/10.12989/gae.2019.17.1.031.

Cho, S.E. (2009), "Probabilistic assessment of slope stability that considers the spatial variability of soil properties", *J. Geotech. Geoenviron. Eng.*, **136**(7), 975-984. https://doi.org/10.1061/(asce)gt.1943-5606.0000309.

Cho, S.E. (2014), "Probabilistic stability analysis of rainfall-induced landslides considering spatial variability of permeability", *Eng. Geol.*, **171**, 11-20. https://doi.org/10.1016/j.enggeo.2013.12.015.

Dahal, R.K., Hasegawa, S., Nonomura, A., Yamanaka, M., Dhakal, S. and Paudyal, P. (2008), "Predictive modelling of rainfall-induced landslide hazard in the lesser himalaya of nepal based on weights-of-evidence", *Geomorphology*, **102**, 496-510. https://doi.org/10.1016/j.geomorph.2008.05.041.

Dai, F. and Lee, C. (2001), "Frequency-volume relation and prediction of rainfall-induced landslides", *Eng. Geol.*, **59**, 253-266. https://doi.org/10.1016/s0013-7952(00)00077-6.

Elkateb, T., Chalaturnyk, R. and Robertson, P.K. (2003), "An overview of soil heterogeneity: Quantification and implications on geotechnical field problems", *Can. Geotech. J.*, **40**, 1-15. https://doi.org/10.1139/t02-090.

Fenton, G.A. and Griffiths, D.V. (2008), *Risk Assessment in Geotechnical Engineering*, John Wiley & Sons.

Galanti, Y., Barsanti, M., Cevasco, A., Avanzi, G.D.A. and Giannecchini, R. (2018), "Comparison of statistical methods and multi-time validation for the determination of the shallow landslide rainfall thresholds", *Landslides*, **15**, 937-952. https://doi.org/10.1007/s10346-017-0919-3.

GEO-SLOPE International Ltd. (2018), Factors Controlling Rainfall-Induced Instability, Example illustrates the importance of some factors that influence the stability of a slope during rainfall. https://www.geoslope.com.

Griffiths, D. and Fenton, G.A. (2004), "Probabilistic slope stability analysis by finite elements", *J. Geotech. Geoenviron. Eng.*, **130**, 507-518. https://doi.org/10.1061/(asce)1090-0241(2004)130:5(507).

Griffiths, D. and Lane, P. (1999), "Slope stability analysis by finite elements", *Geotechnique*, **49**, 387-403. https://doi.org/10.1680/geot.1999.49.3.387.

Griffiths, D., Huang, J. and Fenton, G.A. (2009), "Influence of spatial variability on slope reliability using 2-d random fields", *J. Geotech. Geoenviron. Eng.*, **135**(10), 1367-1378. https://doi.org/10.1061/(asce)gt.1943-5606.0000099.

Guzzetti, F., Peruccacci, S., Rossi, M. and Stark, C.P. (2008), "The rainfall intensity–duration control of shallow landslides and debris flows: An update", *Landslides*, **5**, 3-17. https://doi.org/10.1007/s10346-007-0112-1.

Hu, H. and Huang, Y. (2019), "A dynamic reliability approach to seismic vulnerability analysis of earth dams", *Geomech. Eng.*, **18**(6), 661-668. https://doi.org/10.12989/gae.2019.18.6.661.

Huang, J., Griffiths, D. and Fenton, G.A. (2010), "System reliability of slopes by RFEM", *Soils Found.*, **50**(3), 343-353. https://doi.org/10.3208/sandf.50.343.

Huang, J., Ju, N., Liao, Y. and Liu, D. (2015), "Determination of rainfall thresholds for shallow landslides by a probabilistic and empirical method", *Nat. Hazards Earth Syst. Sci.*, **15**(12), 2715-2723. https://doi.org/10.5194/nhessd-3-3487-2015.

Huang, J., Lyamin, A., Griffiths, D., Krabbenhoft, K. and Sloan, S. (2013), "Quantitative risk assessment of landslide by limit analysis and random fields", *Comput. Geotech.*, **53**, 60-67. https://doi.org/10.1016/j.compgeo.2013.04.009.

Huang, Y. and Xiong, M. (2017), "Dynamic reliability analysis of slopes based on the probability density evolution method", *Soil Dyn. Earthq. Eng.*, **94**, 1-6. https://doi.org/10.1016/j.soildyn.2016.11.011.

Huang, Y., Zhao, L., Xiong, M., Liu, C. and Lu, P. (2018), "Critical slip surface and landslide volume of a soil slope under random earthquake ground motions", *Environ. Earth Sci.*, **77**(23), 1-11. https://doi.org/10.1007/s12665-018-7974-5.

Izadi, A., Jamshidi Chenari, R., Brigid, C. and Javankhoshdel, S. (2020), "Pseudo and full stochastic slope stability analyses using random limit equilibrium method (LEM)", *Proceedings of the GeoCongress*, Minneapolis, Minnesota, U.S.A., February.

Jamshidi Chenari, R. and Alaie, R. (2015), "Effects of anisotropy in correlation structure on the stability of an undrained clay slope", *Georisk Assess. Manage. Risk Eng. Syst. Geohazards*, **9**, 109-123. https://doi.org/10.1080/17499518.2015.1037844.

Jamshidi Chenari, R. and Behfar, B. (2017), "Stochastic analysis of seepage through natural alluvial deposits considering mechanical anisotropy", *Civ. Eng. Infrastruct. J.*, **50**(2), 233-253. https://doi.org/10.7508/ceij.2017.02.003

Javankhoshdel, S., Cami, B., Mafi, R., Yacoub, T. and Bathurst, R.J. (2018), "Optimization techniques in non-circular probabilistic slope stability analysis considering spatial variability", *Proceedings of the GeoEdmonton 2018*, Edmonton, Alberta, Canada, September.

Jiang, S.H. and Huang, J.S. (2016), "Efficient slope reliability analysis at low-probability levels in spatially variable soils", *Comput. Geotech.*, **75**, 18-27. https://doi.org/10.1016/j.compgeo.2016.01.016.

Jiang, S.H., Huang, J. and Zhou, C.B. (2017a), "Efficient system reliability analysis of rock slopes based on subset simulation", *Comput. Geotech.*, **82**, 31-42. https://doi.org/10.1016/j.compgeo.2016.09.009.

Jiang, S.H., Huang, J., Yao, C. and Yang, J. (2017b), "Quantitative risk assessment of slope failure in 2-D spatially variable soils by limit equilibrium method", *Appl. Math. Model.*, **47**, 710-725. https://doi.org/10.1016/j.apm.2017.03.048.

Jiang, S.H., Li, D.Q., Cao, Z.J., Zhou, C.B. and Phoon, K.K. (2014), "Efficient system reliability analysis of slope stability in spatially variable soils using monte carlo simulation", *J. Geotech. Geoenviron. Eng.*, **141**(2), 04014096. https://doi.org/10.1061/(asce)gt.1943-5606.0001227.

Johnson, B.C., Campbell, C.S. and Melosh, H.J. (2016), "The reduction of friction in long runout landslides as an emergent phenomenon", *J. Geophys. Res. Earth Surf.*, **121**, 881-889. https://doi.org/10.1002/2015jf003751.

Juang, C.H., Zhang, J. and Gong, W. (2015), "Reliability-based assessment of stability of slopes", *IOP Conf. Ser. Earth Environ. Sci.*, **26**(1), 012006. https://doi.org/10.1088/1755-1315/26/1/012006.

Klose, M., Damm, B. and Terhorst, B. (2015), "Landslide cost modeling for transportation infrastructures: A methodological approach", *Landslides*, **12**(2), 321-334. https://doi.org/10.1007/s10346-014-0481-1.

Lee, L.M., Gofar, N. and Rahardjo, H. (2009), "A simple model for preliminary evaluation of rainfall-induced slope instability", *Eng. Geol.*, **108**(3-4), 272-285. https://doi.org/10.1016/j.enggeo.2009.06.011.

Li, D.Q., Xiao, T., Cao, Z.J., Phoon, K.K. and Zhou, C.B. (2016b), "Efficient and consistent reliability analysis of soil slope stability using both limit equilibrium analysis and finite element analysis", *Appl. Math. Model.*, **40**(9-10), 5216-5229. https://doi.org/10.1016/j.apm.2015.11.044.

Li, D.Q., Xiao, T., Cao, Z.J., Zhou, C.B. and Zhang, L.M. (2016a), "Enhancement of random finite element method in reliability analysis and risk assessment of soil slopes using subset simulation", *Landslides*, **13**, 293-303. https://doi.org/10.1007/s10346-015-0569-2.

Li, D.Q., Yang, Z.Y., Cao, Z.J., Au, S.K. and Phoon, K.K. (2017), "System reliability analysis of slope stability using generalized subset simulation", *Appl. Math. Model.*, **46**, 650-664. https://doi.org/10.1016/j.apm.2017.01.047.

Li, J. and Chen, J. (2008), "The principle of preservation of probability and the generalized density evolution equation", *Struct. Saf.*, **30**, 65-77. https://doi.org/10.1016/j.strusafe.2006.08.001.

Li, J. and Chen, J. (2009), *Stochastic Dynamics of Structures*, John Wiley & Sons.

Li, L. and Chu, X. (2016), "Risk assessment of slope failure by representative slip surfaces and response surface function", *KSCE J. Civ. Eng.*, **20**(5), 1783-1792. https://doi.org/10.1007/s12205-015-2243-6.

Lin, Q. and Wang, Y. (2018), "Spatial and temporal analysis of a fatal landslide inventory in China from 1950 to 2016", *Landslides*, **15**(12), 2357-2372. https://doi.org/10.1007/s10346-018-1037-6

Liu, L.L., Cheng, Y.M., Wang, X.M., Zhang, S.H. and Wu, Z.H. (2017), "System reliability analysis and risk assessment of a layered slope in spatially variable soils considering stratigraphic boundary uncertainty", *Comput. Geotech.*, **89**, 213-225. https://doi.org/10.1016/j.compgeo.2017.05.014.

Low, B., Lacasse, S. and Nadim, F. (2007), "Slope reliability analysis accounting for spatial variation", *Georisk*, **1**(4), 177-189. https://doi.org/10.1080/17499510701772089.

Mafi, R., Javankhoshdel, S., Cami, B., Jamshidi Chenari, R. and Gandomi, A.H. (2020), "Surface altering optimisation in slope stability analysis with non-circular failure for random limit equilibrium method", *Georisk Assess. Manage. Risk Eng. Syst. Geohazards*, 1-27. https://doi.org/10.1080/17499518.2020.1771739.

Ozbay, A. and Cabalar, A. (2015), "FEM and LEM stability analyses of the fatal landslides at öllolar open-cast lignite mine in elbistan, turkey", *Landslides*, **12**, 155-163. https://doi.org/10.1007/s10346-014-0537-2.

Qi, X.H. and Li, D.Q. (2018), "Effect of spatial variability of shear strength parameters on critical slip surfaces of slopes", *Eng. Geol.*, **239**, 41-49. https://doi.org/10.1016/j.enggeo.2018.03.007.

Rahardjo, H., Ong, T., Rezaur, R. and Leong, E.C. (2007), "Factors controlling instability of homogeneous soil slopes under rainfall", *J. Geotech. Geoenviron. Eng.*, **133**(12), 1532-1543. https://doi.org/10.1061/(asce)1090-0241(2007)133:12(1532).

Segoni, S., Piciullo, L. and Gariano, S.L. (2018), "A review of the recent literature on rainfall thresholds for landslide occurrence", *Landslides*, **15**(8), 1483-1501. https://doi.org/10.1007/s10346-018-0966-4.

Staron, L. and Lajeunesse, E. (2009), "Understanding how volume affects the mobility of dry debris flows", *Geophys. Res. Lett.*, **36**(12). https://doi.org/10.1029/2009GL038229.

Van Genuchten, M.T. (1980), "A closed-form equation for predicting the hydraulic conductivity of unsaturated soils", *Soil Sci. Soc. Amer. J.*, **44**, 892-898. https://doi.org/10.2136/sssaj1980.03615995004400050002x.

Van Tien, P., Sassa, K., Takara, K., Fukuoka, H., Dang, K., Shibasaki, T., Ha, N.D., Setiawan, H. and Loi, D.H. (2018), "Formation process of two massive dams following rainfall-induced deep-seated rapid landslide failures in the kii peninsula of Japan", *Landslides*, **15**, 1761-1778. https://doi.org/10.1007/s10346-018-0988-y.

Vanapalli, S., Fredlund, D., Pufahl, D. and Clifton, A. (1996), "Model for the prediction of shear strength with respect to soil suction", *Can. Geotech. J.*, **33**(3), 379-392. https://doi.org/10.1139/t96-060.

Vanmarcke, E. (1983), *Random Fields*: *Analysis and Synthesis*, MIT Press.

Wang, X., Wang, H. and Liang, R.Y. (2017), "A method for slope stability analysis considering subsurface stratigraphic uncertainty", *Landslides*, **15**(5), 925-936. https://doi.org/10.1007/s10346-017-0925-5.

Xu, C., Xu, X., Shen, L., Yao, Q., Tan, X., Kang, W., Ma, S., Wu, X., Cai, J. and Gao, M. (2016), "Optimized volume models of earthquake-triggered landslides", *Sci. Reports*, **6**(1), 29797. https://doi.org/10.1038/srep29797.

Yang, K.H., Huynh, V.D.A., Nguyen, T.S. and Portelinha, F.H.M. (2018), "Numerical evaluation of reinforced slopes with various backfill-reinforcement-drainage systems subject to rainfall infiltration", *Comput. Geotech.*, **96**, 25-39. https://doi.org/10.1016/j.compgeo.2017.10.012.

Yin, Y., Li, B., Wang, W., Zhan, L., Xue, Q., Gao, Y., Zhang, N., Chen, H., Liu, T. and Li, A. (2016), "Mechanism of the december 2015 catastrophic landslide at the shenzhen landfill and controlling geotechnical risks of urbanization", *Engineering*, **2**(2), 230-249. https://doi.org/10.1016/j.eng.2016.02.005.

Yu, M., Huang, Y., Xu, Q., Guo, P. and Dai, Z. (2016), "Application of virtual earth in 3d terrain modeling to visual analysis of large-scale geological disasters in mountainous areas", *Environ. Earth Sci.*, **75**(7), 563. https://doi.org/10.1007/s12665-015-5161-5.

Zhang, J. and Huang, H. (2016), "Risk assessment of slope failure considering multiple slip surfaces", *Comput. Geotech.*, **74**, 188-195. https://doi.org/10.1016/j.compgeo.2016.01.011.

Zhang, J., Huang, H.W., Zhang, L.M., Zhu, H.H. and Shi, B. (2014), "Probabilistic prediction of rainfall-induced slope failure using a mechanics-based model", *Eng. Geol.*, **168**, 129-140. https://doi.org/10.1016/j.enggeo.2013.11.005

Zhang, J., Zhang, L. and Tang, W.H. (2010), "Slope reliability analysis considering site-specific performance information", *J. Geotech. Geoenviron. Eng.* **137**(3), 227-238. https://doi.org/10.1061/(asce)gt.1943-5606.0000422.

Zhang, L., Zhang, L. and Tang, W. (2005), "Rainfall-induced slope failure considering variability of soil properties", *Geotechnique*, **55**(2), 183-188. https://doi.org/10.1680/geot.55.2.183.59525.

Zhu, J.Q. and Yang, X.L. (2018), "Probabilistic stability analysis of rock slopes with cracks", *Geomech. Eng.*, **16**(6), 655-667. https://doi.org/10.12989/gae.2018.16.6.655.

CC